The 2012 World Congress on
Advances in Civil, Environmental, and Materials Research (ACEM' 12)
Seoul, Korea, August 26-30, 2012

3D Numerical Simulation of Wave forces on an offshore wind turbine foundation

*Sung-Jin Choi[1)], Kwang-Ho Lee[2)], and Ove Tobias Gudmestad[3)]

[1), 3)] *Faculty of Science and Technology, University of Stavanger, Norway*
[2)] *Waterfront and Coastal Research Center, Kwandong University, South Korea*
[1)] *sung-jin.choi@uis.no*

ABSTRACT

A 3D numerical model is developed for simulating wave forces acting on an offshore wind turbine foundation. The model is based on the viscous and incompressible Navier-Stokes equations and uses a volume of fluid method for the displacement of the free surface. A new application, based on the Cut-Cell method, is developed in order to easily install complicated obstacles in a computational domain. The free surface displacements, water particle velocities, dynamic pressures, and inline wave forces are calculated by the numerical model, and the computed results show good agreement with experimental data. From the simulation results, it is concluded that the proposed numerical model is a useful tool which can predict wave forces on an offshore wind turbine foundation.

1. INTRODUCTION

In designing fixed offshore wind turbine foundations, accurate estimation of wave forces acting on them is of great important. To date, conventional methods such as a combination of a wave analysis model and a structural analysis model have mainly been used for estimating wave forces acting on an offshore structure. However, such methods seem to have problems with respect to the accurate estimation of the wave forces. Firstly, the wave analysis models are based on shallow water equations. Although the wave models using the shallow water equations can simulate undisturbed wave kinematics at the structural position to a reasonable degree, they are unlikely to be sufficient for simulating nonlinear interactions between waves and the structure. Secondly, the structural analysis models are based on Morison equation. However, in the Morison equation, inertia and drag coefficients involve uncertainties in their

[2, 3)] Professor
[1)] PhD Student

applications because they were estimated from different experimental studies. Moreover, the coefficients depend greatly on structural shapes. If the shape of each member of the foundation is complex, the coefficients have to be estimated for each member on the basis of additional experimental approaches instead of using the general values presented in recipes such as DnV-RP-C205 (2007).

A Navier-Stokes solver is an alternative method for overcoming such problems. Because the Navier-Stokes solver can not only specifically simulate nonlinear characteristics of the waves occurring in the vicinity of the complex structure but also calculate the wave forces by integrating directly the pressures along the structure surface, there is no need to employ an empirical formula such as the Morison equation and an additional wave analysis model for computing the wave forces on the structure.

The main objective of this study is to propose a 3D numerical model which can directly predict wave forces on a cylindrical pile without the use of an empirical formula and an additional wave analysis model. In order to achieve the purpose of the present study, a 3D Navier-Stokes solver, based on viscous and incompressible momentum equations for a two-phase flow (water and air) model and the VOF (Volume of Fluid) method (Hirt and Nichols,1981), is used. The cylindrical pile in the computational domain is calculated by a new application based on Cut-Cell method. The free surface elevation, horizontal water particle velocities, dynamic pressures, and wave forces on the cylindrical pile are calculated by the numerical model, and the calculated results are compared with experimental data presented by Mo et al. (2007) to confirm accuracy of the numerical model.

2. NUMERICAL MODEL

When a fluid is modeled as a viscous and incompressible fluid with constant density, the fluid motion can be described by the continuity equation (Eq. 1) and the modified Navier-Stokes equations (Eqs. 2 to 4).

$$\frac{\partial(m_x u)}{\partial x}+\frac{\partial(m_y v)}{\partial y}+\frac{\partial(m_z w)}{\partial z}=q^* \tag{1}$$

$$\begin{aligned} &m_v\frac{\partial u}{\partial t}+m_x u\frac{\partial u}{\partial x}+m_y v\frac{\partial u}{\partial y}+m_z w\frac{\partial u}{\partial z}\\ &\quad=-\frac{m_v}{\hat{\rho}}\frac{\partial p}{\partial x}+\frac{\partial}{\partial x}\{m_x(-\tau_{xx}+2\hat{\nu}D_{xx})\}+\frac{\partial}{\partial y}\{m_y(-\tau_{xy}+2\hat{\nu}D_{xy})\}\\ &\quad+\frac{\partial}{\partial z}\{m_z(-\tau_{xz}+2\hat{\nu}D_{xz})\}+\frac{F_s}{\hat{\rho}}-\frac{2m_x\hat{\nu}}{3}\frac{\partial q^*}{\partial x} \end{aligned} \tag{2}$$

$$\begin{aligned} &m_v\frac{\partial v}{\partial t}+m_x u\frac{\partial v}{\partial x}+m_{vy} v\frac{\partial v}{\partial y}+m_z w\frac{\partial v}{\partial z}\\ &\quad=-\frac{m_v}{\hat{\rho}}\frac{\partial p}{\partial y}+\frac{\partial}{\partial x}\{m_x(-\tau_{yx}+2\hat{\nu}D_{yx})\}+\frac{\partial}{\partial y}\{m_y(-\tau_{yy}+2\hat{\nu}D_{yy})\}\\ &\quad+\frac{\partial}{\partial z}\{m_z(-\tau_{yz}+2\hat{\nu}D_{yz})\}+\frac{F_s}{\hat{\rho}}-\frac{2m_y\hat{\nu}}{3}\frac{\partial q^*}{\partial y} \end{aligned} \tag{3}$$

$$m_v \frac{\partial w}{\partial t} + m_x u \frac{\partial w}{\partial x} + m_y v \frac{\partial w}{\partial y} + m_z w \frac{\partial w}{\partial z}$$
$$= -\frac{m_v}{\hat{\rho}} \frac{\partial p}{\partial z} + \frac{\partial}{\partial x}\{m_x(-\tau_{zx} + 2\hat{\nu} D_{zx})\} + \frac{\partial}{\partial y}\{m_y(-\tau_{zy} + 2\hat{\nu} D_{zy})\}$$
$$+ \frac{\partial}{\partial z}\{m_z(-\tau_{zz} + 2\hat{\nu} D_{zz})\} + \frac{F_s}{\hat{\rho}} - \frac{2 m_z \hat{\nu}}{3} \frac{\partial q^*}{\partial z} - m_v g - \lambda w \quad (4)$$

Where, t is the time, p is the pressure, u, v, and w are the velocity components in each directions, M_v is the ratio of the fractional volume open to the flow, M_x, M_y, M_z are the ratio of the fractional area open to the flow in each directions, τ_{ij} is the turbulent stress based on the Smagorinsky SGS model (Smagorinsky, 1963), D_{ij} is the stress rate tensor, F_s is the surface tension force based on the CSF (Continuum Surface Force) model, λ is the wave dissipation factor that equals 0 except in the added dissipation zone, $\hat{\rho}$ is the fluid density, $\hat{\nu}$ is the fluid kinematic molecular viscosity, and q^* is the source term required to generate waves assigned only at the source position ($x = x_s$), defined as $q^* = q(z,t)/\Delta x_s$, where q is the flux density and Δx_s is the mesh width at the source position.

The volume of fluid (VOF) method, which was developed by Hirt and Nichols (1981), is applied to track the interface between two-phase flows. In the VOF method, the interface between the water and the air can be determined by a VOF function (F) which represents the volume of fluid in a numerical cell. The advection of the VOF function is obtained by solving the conservation of fluid mass in each cell as follows;

$$\frac{\partial (m_v F)}{\partial t} + \frac{\partial (m_x u F)}{\partial x} + \frac{\partial (m_y v F)}{\partial y} + \frac{\partial (m_z w F)}{\partial z} = F q^* \quad (5)$$

To solve the above governing equations (eqs. 1 to 5) numerically, a fixed rectangular grid system is used in the computational domain. However, in the case that a complicated obstacle is installed within the computational domain, the obstacle cannot be exactly expressed by the rectangular cells and, furthermore, surfaces of discontinuity occurring by the rectangular cells can impinge on calculation of wave and flow fields in the vicinity of the obstacle. In order to overcome the problems of incorporating complicated obstacles in the computational domain, a new application (Fig. 1), in this study, is developed based on Cut-Cell method, which is similar to the FAVOR method (Fraction Area / Volume Obstacle Representation Method, Hirt and Sicilian (1985)). In the application, four parameters (i.e., m_v: ratio of fractional volume open to flow, m_x, m_y, m_z : ratio of fractional areas open to flow in each directions), the area of the wetted surface of the structure, and the surface unit normal vectors are recorded in each cell. The governing equations (eqs. 1 to 5) are formulated in terms of the computed four parameters to block portions of each cell containing the obstacle. Moreover, the calculated areas of the wetted surface of the structure and surface unit normal vectors are used in order to obtain the wave forces on the structure.

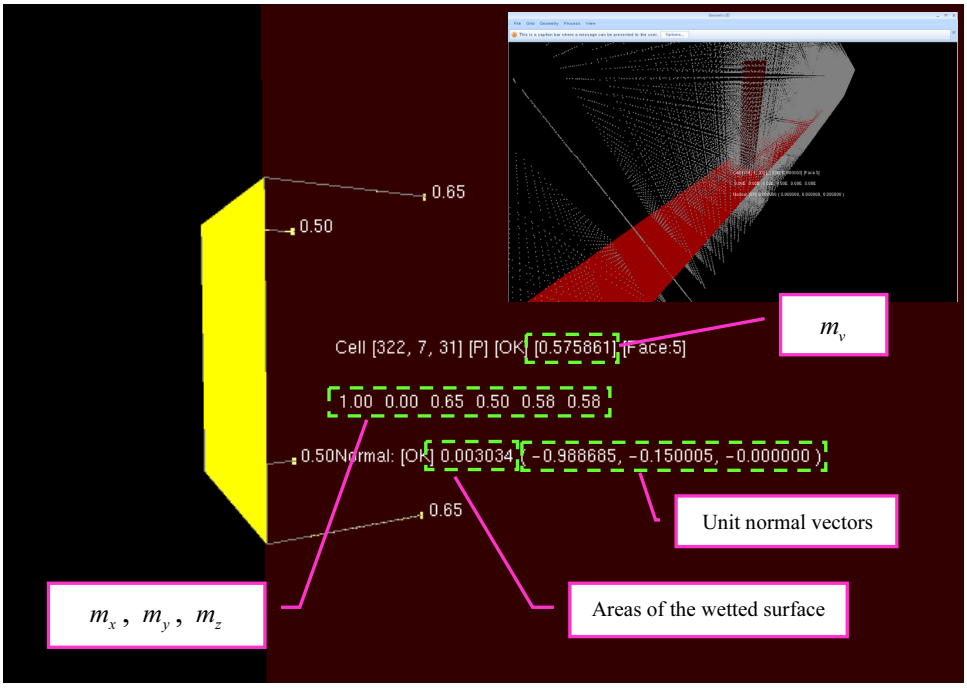

Fig. 1. Calculated results (four parameters (m_v , m_x , m_y , and m_z), the area of the wetted surface of the structure, and the unit normal vectors) by the new application.

Finite difference methods are used to calculate the governing equations and the advection equation for the VOF function. Variables are staggered, which means that the pressure (p), the wave source function (q^*), and the VOF function (F) are computed at the cell center, while the velocity components u , v , w are computed at the center of cell face. The continuity equation is discretized by the central difference method. As for the discretization of the momentum equations, the forward difference method for time derivative terms, a Constrained Interpolation Profile (CIP) for the advection terms, and the central difference method for the non-advection terms are employed, respectively. In the computation, the velocity components (u , v , w) and the pressure p at the new time step is solved using the AP-AMG (Algebraic Multigrid) solver developed by Iwamura (Allied Engineering, 2011). Then, the new free surface configuration is tracked by solving the advection equation for the VOF function, using the updated velocity components.

Appropriate boundary conditions have to be determined to numerically solve the governing equations. As for the free surface boundary conditions, because the water and the air phase are modeled as a fluid in the two-phase flow model, there is no need to apply the dynamic boundary condition at the interface between the air and the water. The dynamic boundary condition is automatically satisfied. On the other hand, the kinematic boundary condition is satisfied by tracking the VOF function. As for the open boundary conditions, added fictitious dissipation zones, such as are proposed by Hinatsu (1992), are located at the end of both sides of the computational domain to absorb wave energy. For a top boundary condition, the pressure-constant condition is applied. An impermeable condition (for normal velocities) and a slip condition (for

tangential velocities) are imposed to treat the bottom boundary condition and the obstacle boundary condition, respectively.

3. APPLICATION OF THE NUMERICAL ANALYSIS

3.1. Numerical wave tank set-up

A numerical wave tank (NWT) similar to an experimental configuration is developed. Fig. 2. shows the schematic sketch of the numerical wave tank. The length, the width, and the height of the numerical wave tank are 31 m, 5 m, and 7 m, respectively. In the numerical wave tank (NWT), the computational domain is discetized using non-uniform grids with mesh size Δx = 0.05 - 0.1 m in the x-direction, Δy = 0.05 ~ 0.1 m in the y-direction, and Δz = 0.1 ~ 0.2 m in the z-direction. The Still Water Level (SWL) is at 4.76 m above the bottom. Added fictitious dissipation zones are located to the left and right sides of the computational domain with a thickness of 2L (L is the wave length) to absorb the wave energy. An internal wave generator, which can generate a regular wave train using Stream function wave theory, is located in front of the added fictitious dissipation which is located at the left part of the computational domain. A cylindrical pile with a diameter of 0.7 m is located 27.5 m away from the internal wave generator. An incident deterministic wave condition (wave height H_I = 1.2 m and wave period T = 4.0 sec) is considered. The model is run for 40 seconds (i.e., 10 wave periods).

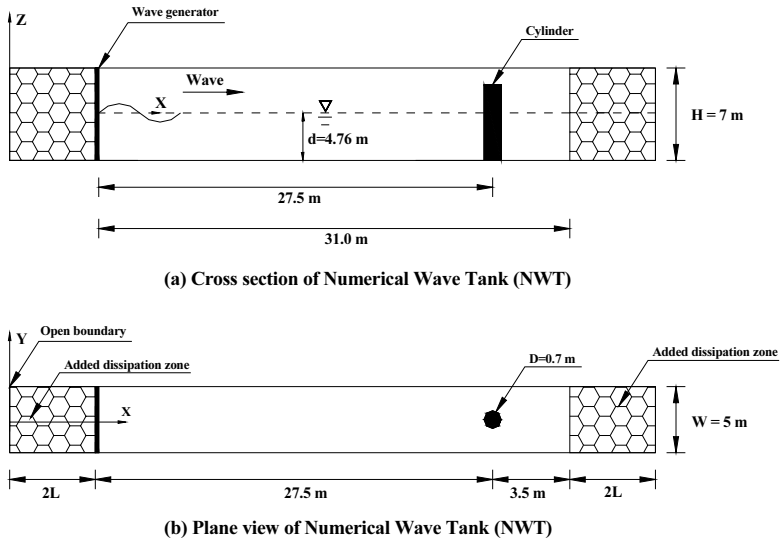

Fig. 2. Cross section (a) and plane view (b) of the Numerical Wave Tank (NWT)

3.2. Results and discussions

3.2.1 Free surface elevation

Figs. 4 to 6 show the comparison between the calculated and the measured free surface elevation at WG1, WG 2, and WG 3. Three wave gauges are located in front of

the pile (WG 1), at the right side of the pile (WG 2), and at the rear side of the pile (WG 3), respectively (Fig. 3.). In addition, a reference wave gauge (WG 11) is located at the side wall of the wave tank corresponding to the front line of the pile. The free surface displacements which are measured at all gauges are normalized by the maximum free surface elevation at WG 11. In these figures, the black lines represent the computed free surface elevations and the red open circles indicate the measured free surface elevations. As shown in the Figs. 4 to 6, an excellent agreement between the measured and the calculated free surface elevations is observed.

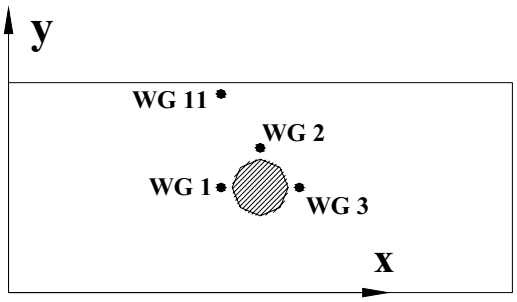

Fig. 3. Locations of wave gauges (WG 11, WG 1, WG 2, and WG 3)

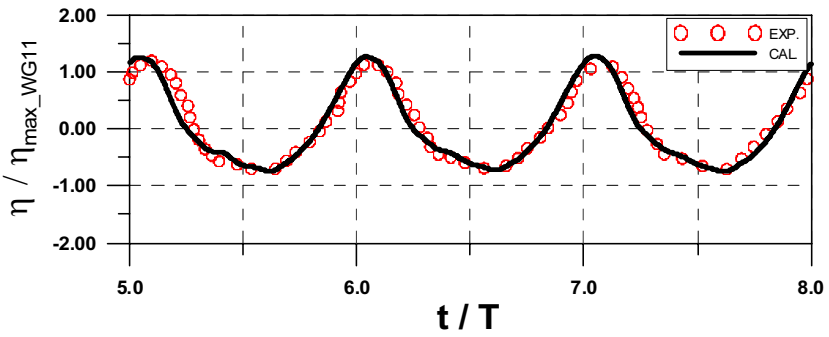

Fig. 4. Free surface elevations from experimental data (EXP.) and computed by the Navier-Stokes solver (CAL.) at WG 1

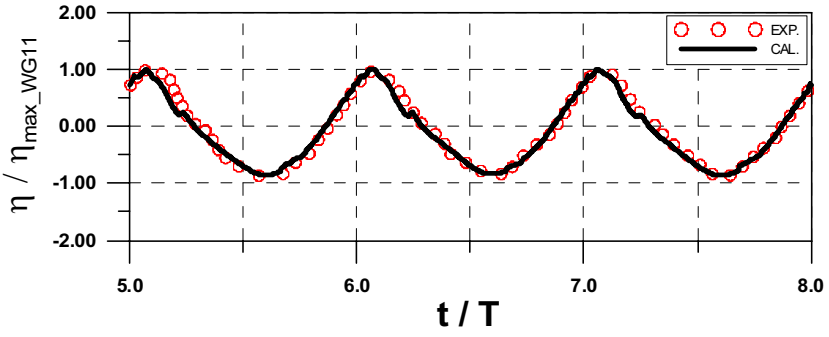

Fig. 5. Free surface elevations from experimental data (EXP.) and computed by the Navier-Stokes solver (CAL.) at WG 2

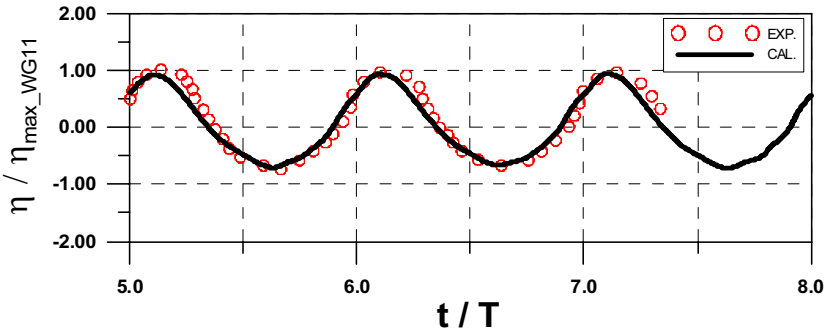

Fig. 6. Free surface elevations from experimental data (EXP.) and computed by the Navier-Stokes solver (CAL.) at WG 3

Fig. 7. shows a snapshot of the spatiotemporal variations of an instantaneous water level (time= 31.54 sec). The wave-structure interaction occurring in the vicinity of cylindrical pile is simulated well in the computational domain.

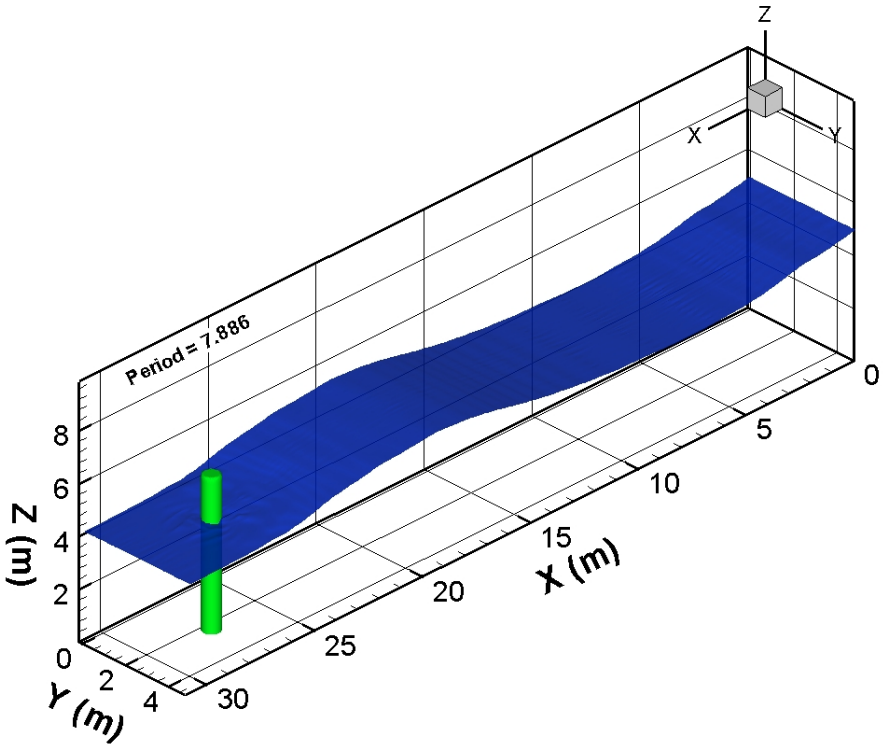

Fig. 7. Snapshot of the spatiotemporal variations of an instantaneous water level (time= 31.54 sec)

3.2.2 Horizontal water particle velocity

Figs. 9 to 11 compare the calculated horizontal water particle velocities with the measured horizontal water particle velocities at three ADV meters (ADV 1 to 3). The ordinate in the figures is the horizontal velocity normalized by wave celerity (C). The ADV meters (and propeller probes) are located at different elevations on the side wall of the wave tank corresponding to the front line of the pile (Fig. 8.). According to the

results of the three ADV meters (ADV 1 to 3), the velocities calculated by the Navier-Stokes solver agree very well with the measured velocities.

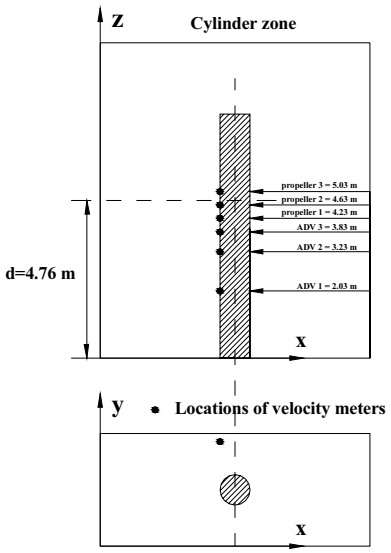

Fig. 8. Locations of velocity meters (ADV 1 to 3 and Propeller 1 to 3)

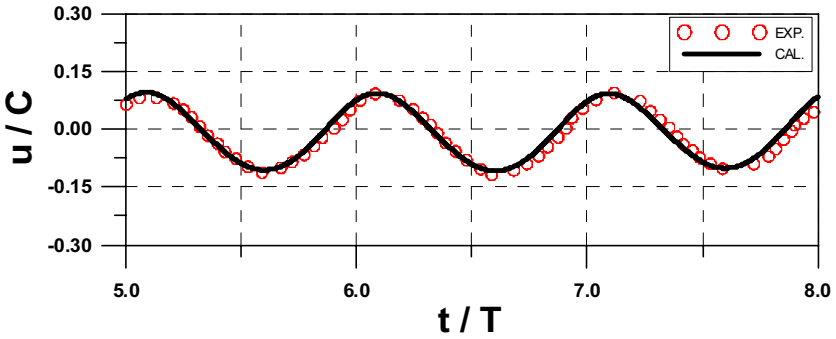

Fig. 9. Horizontal water particle velocities from experimental data (EXP.) and computed by the Navier-Stokes solver (CAL.) at ADV 1

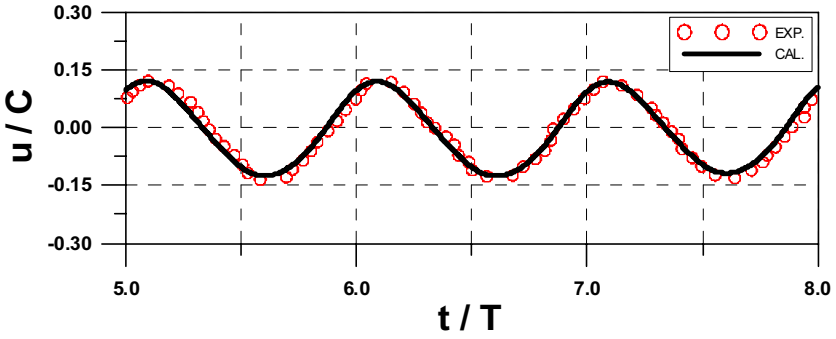

Fig. 10. Horizontal water particle velocities from experimental data (EXP.) and computed by the Navier-Stokes solver (CAL.) at ADV 2

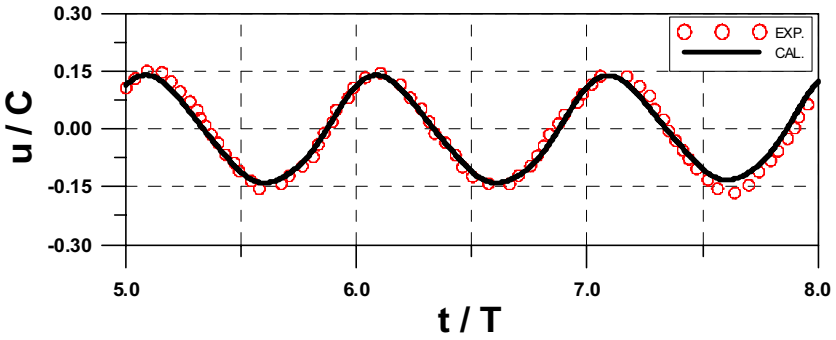

Fig. 11. Horizontal water particle velocities from experimental data (EXP.) and computed by the Navier-Stokes solver (CAL.) at ADV 3

The computed water particle velocities and the velocities measured by the propeller probes are compared in Figs. 12, 13, and 14. A reasonable agreement between the measured and the calculated velocities are observed although the calculated results at the crests are somewhat underestimated compared with the measured results. It should be noted that the propeller probes can only measure the absolute values of the horizontal water particle velocities, as shown in Fig. 12. A discrepancy between measured and computed results at non-dimensional time (e.g., $5.4 \leq t/T \leq 5.8$) in Figs. 13 and 14 is observed. The discrepancy would be explained as follows. The used CFD model is based on the two-phase (water and air) model, which means that the air and the water velocities are calculated simultaneously in each cell. Therefore, even for the case that the progressive waves do not hit the propeller probes (i.e., forms the wave trough, $5.4 \leq t/T \leq 5.8$), the velocities can be calculated in each cell, contrary to the measured results at the propeller probes (i.e., the measured velocities are zero). It is thought that the calculated velocities at the non-dimensional time (e.g., $5.4 \leq t/T \leq 5.8$) are the air velocities.

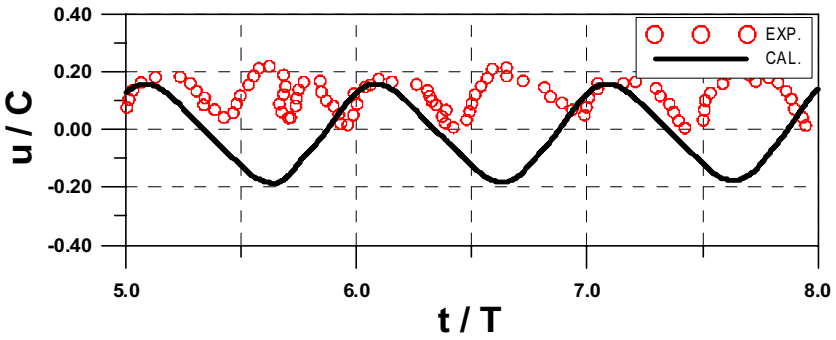

Fig. 12. Horizontal water particle velocities from experimental data (EXP.) and computed by the Navier-Stokes solver (CAL.) at Propeller 1

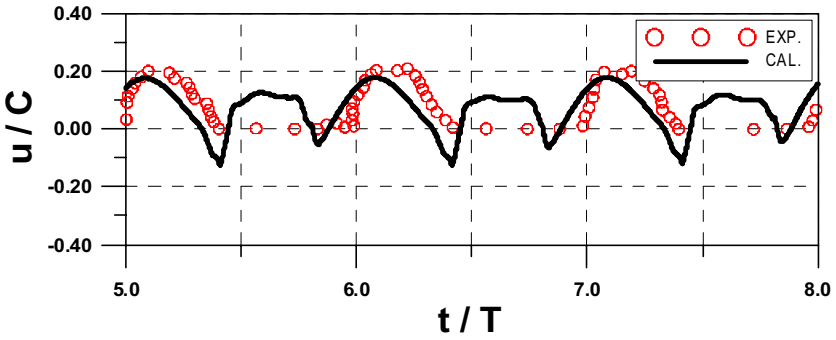

Fig. 13. Horizontal water particle velocities from experimental data (EXP.) and computed by the Navier-Stokes solver (CAL.) at Propeller 2

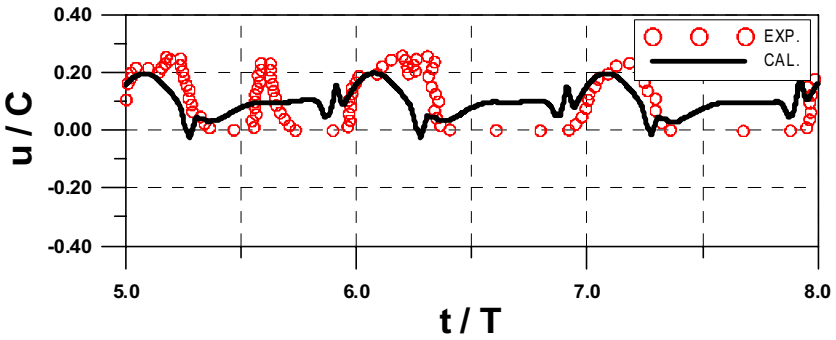

Fig. 14. Horizontal water particle velocities from experimental data (EXP.) and computed by the Navier-Stokes solver (CAL.) at Propeller 3

3.2.3 Dynamic pressures

The computed and the measured dynamic pressures at a horizontal cross section are compared in Figs. 16 to 18. The dynamic pressures which are measured at all gauges are normalized by the hydrostatic pressure (ρgH). The pressure cells are spread out over the circumference ($\theta = 0^\circ$, $\theta = 90^\circ$, and $\theta = 180^\circ$) at 4.23 m over the bottom of the tank (Fig. 15.). The agreement between the computed results and the measured results is good although there is only a small gap between the calculated and the measured dynamic pressures at the pressure trough in $\theta = 180^\circ$ (Fig. 18.).

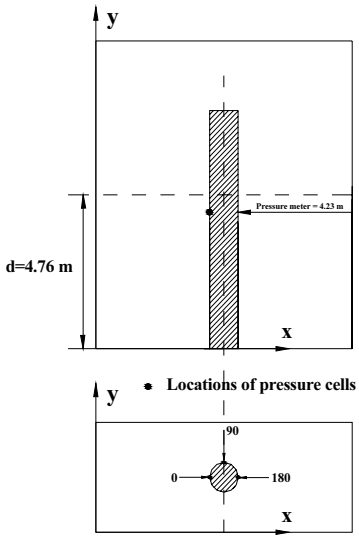

Fig. 15. Locations of pressure cells ($\theta = 0^{\circ}$, $\theta = 90^{\circ}$, and $\theta = 180^{\circ}$)

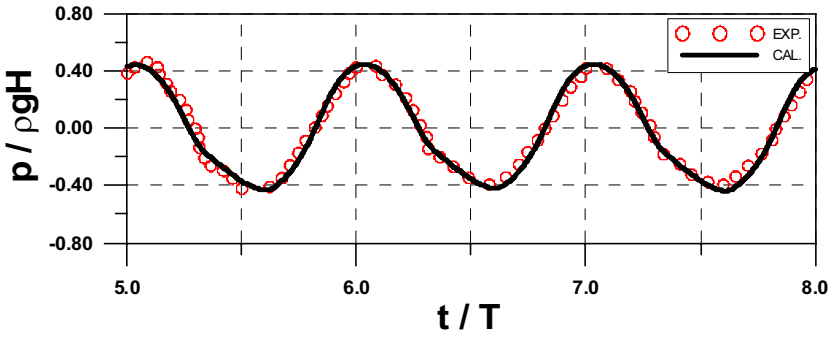

Fig. 16. Dynamic pressures from experimental data (EXP.) and computed by the Navier-Stokes solver (CAL.) at a horizontal cross section ($\theta = 0^{\circ}$)

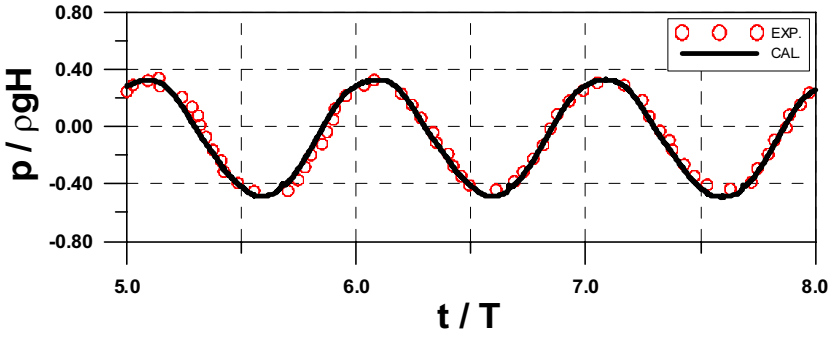

Fig. 17. Dynamic pressures from experimental data (EXP.) and computed by the Navier-Stokes solver (CAL.) at a horizontal cross section ($\theta = 90^{\circ}$)

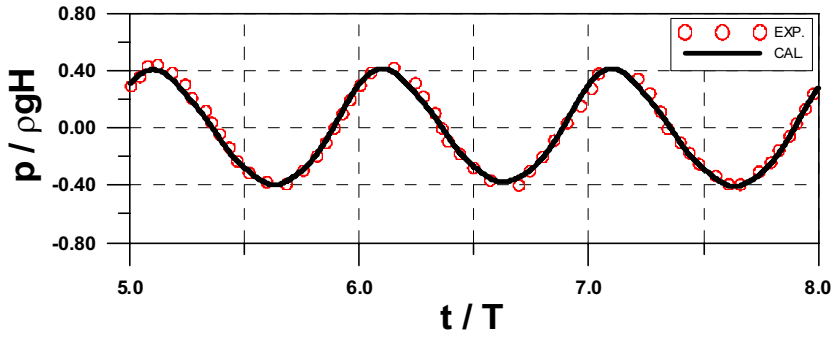

Fig. 18. Dynamic pressures from experimental data (EXP.) and computed by the Navier-Stokes solver (CAL.) at a horizontal cross section ($\theta = 180^{\circ}$)

3.2.4 Wave forces on a cylindrical pile

The measured inline wave forces and the inline wave forces calculated by the Navier-Stokes solver are compared in Fig. 19. The ordinate in the figures is the inline wave forces on the cylindrical pile normalized by $\rho g D H^2$ .The computed inline wave forces are obtained by integrating the fluid pressures on the wetted surface of the cylindrical pile. The comparison reveals that the time variations of the computed inline wave forces are very similar to the time variations of the measured inline wave forces although there is a small discrepancy at the troughs of the wave forces. The small discrepancy would be attributed to the shape of the cylindrical pile depicted in the each wave tank. The cylindrical pile which is used in the experiments is a true circle, but the cylindrical pile which is employed in the computational domain is a polygon which is split in an arbitrary number. Even though the new application based on the Cut-Cell method is employed in order to correctly approximate the structure in the computational domain, the slight difference between experiments and numerical analysis would result in a slightly underestimated wave forces in the trough in the numerical simulation. The discrepancy can be improved by using finer grids, but this would lead to long time simulation.

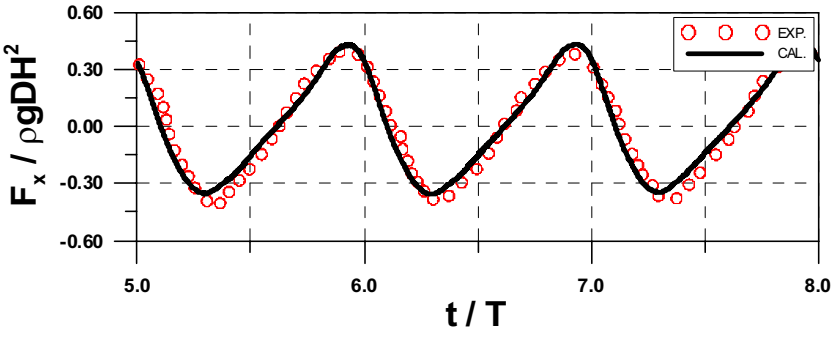

Fig. 19. Inline wave forces from experimental data (EXP.) and computed by the Navier-Stokes solver (CAL.)

4. CONCLUSION

Free surface elevation, the horizontal water particle velocities, the dynamic wave pressures, and the inline wave forces on a cylindrical pile installed on a flat bottom are calculated by a proposed 3D numerical model, and the computed results are compared with the experimental data presented by Mo et al. (2007). The numerical model shows very good performance in estimating the free surface elevation, the horizontal water particle velocities, and the dynamic pressures in the vicinity of the cylindrical pile. Moreover, the computed inline wave forces agree very well with the measured results although the inline forces around the trough are slightly underestimated compared with the measured values. Therefore, the proposed numerical model can be used as a useful tool for predicting the wave forces on an offshore wind turbine foundation without the use of an empirical formula and an additional wave analysis model.

ACKNOWLEDGEMENTS

The research was supported by a grant (“stipendiat-TN-2008”) from the Research Council of Norway. The AP-AMG solver for solving Poisson Pressure Equation (PPE) was provided by Chihiro Iwamura, Allied Engineering Corporation, Japan

REFERENCES

Allied Engineering, User’s Manual for Advanced Parallel AMG Version 1.3, Tokyo,2011.
DnV-RP-C205, Recommended Practice, Environmental Conditions and Environmental Loads, 44, 52-53, DET NORSKE VERITAS, Oslo, Norway, 2007.
Hinatsu M (1992). Numerical simulation of unsteady viscous nonlinear waves using moving grid systems fitted on a free surface. J. Kansai Soc. Naval Archit. Jpn. 217:1 -11.
Hirt CW, and Nichols BD. (1981), Volume of fluid method for the dynamics of free boundaries. Journal of Computational Physics 39(1):201-225.
Hirt CW, Sicilian JM (1985). A porosity technique for the definition of obstacles in rectangular cell meshes. Proceedings of the 4th International conference on Numerical Ship Hydrodynamics, Washington D.C., 1-10.
Mo W, Irschik K, Oumeraci H, Liu PL-F (2007). A 3D numerical model for computing non-breaking wave forces on slender piles. Journal of Engineering Mathematics 58:19 -30.
Smagorinsky J (1963). General circulation experiments with the primitive equation. Monthly Weather Review 91(3):99-164.